DOI: 10.1002/anie.201307581

Integrated Devices

Fiber-Based Flexible All-Solid-State Asymmetric Supercapacitors for Integrated Photodetecting System**

Xianfu Wang, Bin Liu, Rong Liu, Qiufan Wang, Xiaojuan Hou, Di Chen, Rongming Wang,* and Guozhen Shen**

Abstract: *Integrated nanodevices with the capability of storing energy are widely applicable and have thus been studied extensively. To meet the demand for flexible integrated devices, all-solid-state asymmetric supercapacitors that simultaneously realize energy storage and optoelectronic detection were fabricated by growing Co_3O_4 nanowires on nickel fibers, thus giving the positive electrode, and employing graphene as both the negative electrode and light-sensitive material. The as-assembled integrated systems were characterized by an improved energy storage, enhanced power density (at least by 1860 % enhanced) by improving the potential window from 0–0.6 V to 0—1.5 V, excellent photoresponse to white light, and superior flexibility of both the fiber-based asymmetric supercapacitor and the photodetector. Such flexible integrated devices might be used in smart and self-powered sensory, wearable, and portable electronics.*

The fabrication of integrated nanodevices, such as nanogenerators combined with metal-ion-based and wireless detectors,[1,2] and photoelectric converters with the capability to store energy,[3–5] has been explored extensively in recent years because of the diversified function of these devices in comparison to conventional nanodevices with their limited applicability. Integrated photodetectors have drawn great attention because of their importance for specific applications, including environmental monitoring with large-area wireless sensor networks, chemical and biosensing, and in situ monitoring of medical therapy.[6] As they can be operated without an external power source, the extra weight of the latter can be avoided.[7–10] Integrated devices that contain photodetectors are generally planar, which may limit their practical applications. In this regard, a fiber-based device may have unique advantages.[11] The development of flexible integrated photodetectors on single fibers to be used in flexible, wearable, and stretchable electronics is therefore desirable.

High-performance energy storage and supply is indispensable in order to power integrated nanosensors effectively. Supercapacitors have attracted tremendous interest as promising energy-storage devices because of their high power density and their capability to quickly charge and discharge, which are favorable characteristics of devices that are used in hybrid vehicles, portable electronics, and backup energy systems.[12–18] However, most conventional supercapacitors are too heavy and bulky to power nanosensors in small, lightweight, and flexible integrated systems. In recent years, the development of high-performance fiber-based miniaturized supercapacitors has been explored extensively to meet the growing demand for flexible and wearable electronics.[19–24] However, until now, all reported fiber-based supercapacitors were studied only as single-component energy-storage devices, and it is still a great challenge to combine high-performance fiber-based microscale supercapacitors with nanosensors to obtain high-performance fiber-based flexible integrated systems.

Herein, we report the successful fabrication of a fiber-based flexible integrated device for simultaneous energy storage and optoelectronic detection. In this integrated system, a fiber-based flexible all-solid-state asymmetric supercapacitor, which was fabricated using titanium wire/Co_3O_4 nanowires and carbon fibers/graphene electrodes, was used as energy-storage and energy-supply device with a two-dimensional graphene layer as the light-sensitive material. The as-assembled integrated system featured improved energy storage and power delivery (at least by 1860 % enhanced) by improving the potential window from 0–0.6 V to 0–1.5 V, excellent photoresponse to white light, and superior flexibility of both the fiber-based asymmetric supercapacitor and the photodetector.

For the fabrication of fiber-shaped asymmetric supercapacitors, a facile solvothermal method was used to grow porous Co_3O_4 nanowires nickel fibers.[25] Figure 1 a shows the XRD pattern of the as-prepared nanowires scraped off the fibers, which can be indexed to pure Co_3O_4 with cubic structure (JCPDS No. 042-1467). Figure 1 b depicts a typical

[*] X. F. Wang, B. Liu, R. Liu, Q. F. Wang, X. J. Hou, Prof. D. Chen
Wuhan National Laboratory for Optoelectronics (WNLO) and School of Optical and Electronic Information
Huazhong University of Science and Technology (HUST)
Wuhan, 430074 (China)
E-mail: dichen@mail.hust.edu.cn
X. F. Wang, B. Liu, Prof. G. Z. Shen
State Key Laboratory for Superlattices and Microstructures
Institution of Semiconductors, Chinese Academy of Science
Beijing, 100083 (China)
E-mail: gzshen@semi.ac.cn
Prof. R. M. Wang
Key Laboratory of Micro-nano Measurement-Manipulation and Physics (Ministry of Education), Department of Physics
Beijing University of Aeronautics and Astronautics
Beijing 100191 (China)
E-mail: rmwang@buaa.edu.cn

[**] We acknowledge the support from the National Natural Science Foundation (91123008, 61377033), the 973 Program of China (2011CB933300), the Program for New Century Excellent Talents of the University in China (grant no. NCET-11-0179), and the Wuhan Science and Technology Bureau (20122497).

Supporting information for this article is available on the WWW under http://dx.doi.org/10.1002/anie.201307581.

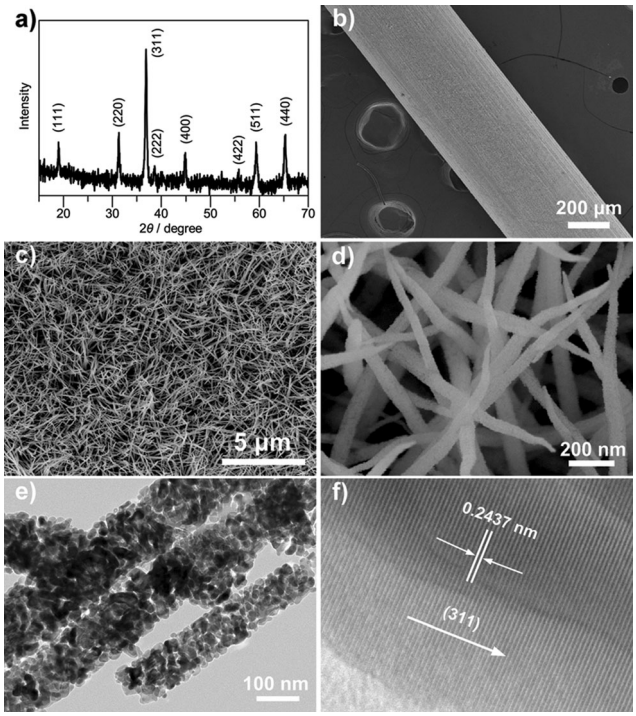

Figure 1. a) XRD pattern of Co_3O_4 scraped off a nickel fiber. b–d) SEM images of the as-synthesized Co_3O_4 nanowires on a nickel fiber. e) TEM, and f) HRTEM images of the Co_3O_4 nanowires.

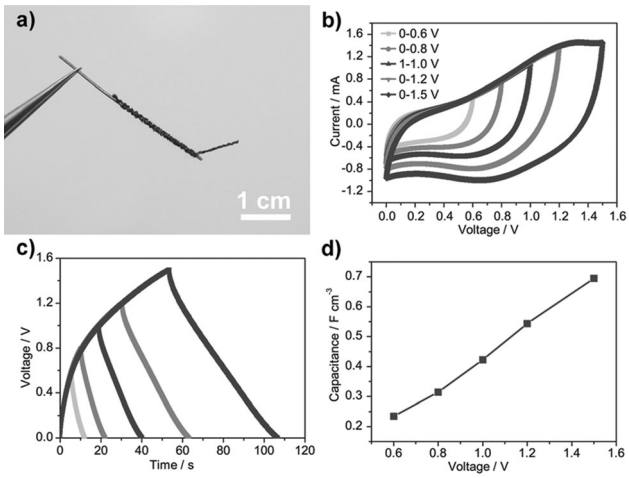

Figure 2. a) Photograph of the fiber-based all-solid-state asymmetric supercapacitor. b) CV curves, c) galvanostatic charge–discharge curves, and d) volumetric capacitances of the asymmetric supercapacitor with the increase of the potential window.

scanning electron microscopy (SEM) image of the nickel fiber/Co_3O_4 nanowires, showing that the nickel fiber was uniformly coated with Co_3O_4 nanowires. Figure 1c,d shows the three-dimensional (3D) nanostructures of the porous Co_3O_4 nanowires, which have a diameter of 50–100 nm and a length of 1–2 μm (Figure S1), grown regularly on the nickel fibers. The existence of porous Co_3O_4 nanowires was further confirmed by transmission electron microscopy (TEM). The TEM image of the nanostructures scraped off the nickel fiber shows that the nanowires are composed of numerous nanocrystals with diameters of 10–20 nm and contain many widely distributed mesopores (Figure 1e). The lattice spacing of 0.2437 nm corresponded to the (311) crystal planes of the cubic Co_3O_4 phase, (see high-resolution TEM (HRTEM) image in Figure 1f). The selected-area electron diffraction (SAED) pattern in Figure S2 (Supporting Information) shows the polycrystalline structure of the Co_3O_4 nanowires. The porous 3D Co_3O_4 nanowires on the nickel fiber possess a large, electrochemically active surface and short paths for fast ion diffusion and electron transport.[26,27] Thus, we were able to employ them as the positive electrode of a supercapacitor to enhance its energy-storage performance.

The electrochemical properties of the as-grown porous Co_3O_4 nanowires on nickel fibers and graphene-coated carbon fibers were first investigated in a three-electrode system with a 6 M KOH electrolyte solution, and both exhibited excellent energy-storage performance (see the Supporting Information, Figures S3–S7). Based on these results, microscale fiber-based all-solid-state asymmetric supercapacitors were prepared from nickel fiber/Co_3O_4 nanowires (positive electrode) and carbon fibers/graphene (negative electrode), to improve energy storage and power delivery (Figure 2a). The fiber-based all-solid-state asymmetric supercapacitors were fabricated by carefully entangling a bundle of carbon fibers coated with graphene around the nickel fiber coated with Co_3O_4 nanowires previously immersed in the PVA-KOH gel solution. The advantage of the asymmetric configuration is the use of the pseudocapacitive positive electrode to enhance the specific capacitance. Besides, the operating potential of the asymmetric cell can be extended as a result of the overpotential of reversible hydrogen electrosorption in a nanoporous carbon-based negative electrode.[28–30] We investigated the cell voltage of the asymmetric supercapacitor by performing a cyclic voltammetry (CV) measurement in a three-electrode cell separately with nickel fiber/Co_3O_4 nanowires and carbon fibers/graphene. A stable potential window was observed in the range from −1.0 to −0.3 V for carbon fibers/graphene and in the range from 0.0 to 0.5 V for nickel fiber/Co_3O_4 nanowires (Figure S8), thus demonstrating that the asymmetric supercapacitor can be operated up to 1.5 V. On the basis of the specific capacitance values and potential windows found for both electrodes, the mass ratio of the negative electrode (carbon fibers/graphene) and the positive electrode (nickel fiber/Co_3O_4 nanowires) was fixed close to 1:0.576. Figure 2b shows a series of CV measurements of the asymmetric supercapacitor with different cell voltages varying from 0.0–0.6 V to 0.0–1.5 V. When the operating potential is 1.0 V, the presence of redox peaks (in the region between 0.0 and 1.0 V) indicates that the pseudocapacitive properties of the cell originate from the positive electrode (nickel fiber/Co_3O_4 nanowires). With an increase of the operating potential to 1.5 V, more Faradic reactions (the larger peak current) occurred. Moreover, the charge–discharge curves of the fiber-shaped all-solid-state asymmetric supercapacitor at a current density of 40 mA cm^{-3} stayed nearly symmetric at an operating potential as high as 1.5 V (Figure 2c), thus suggesting that the device exhibits ideal capacitive characteristics with a rapid I–V response and small equivalent series

resistance.[31] Figure 2d shows a variation of the volumetric capacitance of the asymmetric supercapacitor with an increasing potential window. The volumetric capacitance increases significantly from 0.234 to 0.695 F cm^{-3} with an increase of the operating potential from 0.6 to 1.5 V, thus demonstrating that the amount of stored energy and delivered power can be increased at least by 1860% according to $E = CV^2/2$ compared with that of the supercapacitor with a potential window of 0—0.6 V. The considerably improved energy density can probably be ascribed to the high voltage and the increased capacitance because of Faradaic reactions.

CV curves at different scan rates (ranging from 10 to 100 mV s^{-1}) were also measured below 1.5 V (Figure 3a). Unlike the three-electrode electrochemical feature of nickel fiber/Co_3O_4 nanowires electrodes, the asymmetric device displays a quasi-rectangular CV geometry with feeble redox peaks, thus indicating a combination of both pseudocapacitive and EDLC-type (EDLC = electric double-layer capacitor) properties at all scan rates. Moreover, at a scan rate as high as 100 mV s^{-1} and a maximum cell voltage of 1.5 V, the shape of the CV curve can still be well persevered, thus suggesting a good rate capability of the asymmetric supercapacitor. Galvanostatic discharge curves of the fiber-shaped asymmetric supercapacitor at various current densities are shown in Figure 3b. The volumetric capacitance, which was calculated based on the total volume of the device, reached 2.1 F cm^{-3} at a current density of 20 mA cm^{-3}, and the corresponding specific capacitance was also plotted (see Figure S9). The voltage drop of the asymmetric device versus the charge–discharge current density is shown in Figures S10 and S11, and the corresponding linear functions were fitted. Obviously, the device exhibits pretty low internal resistance, even at a current density as high as 100 mA cm^{-3}, thus showing the excellent electrochemical performance of the fiber-shaped all-solid-state asymmetric supercapacitor.

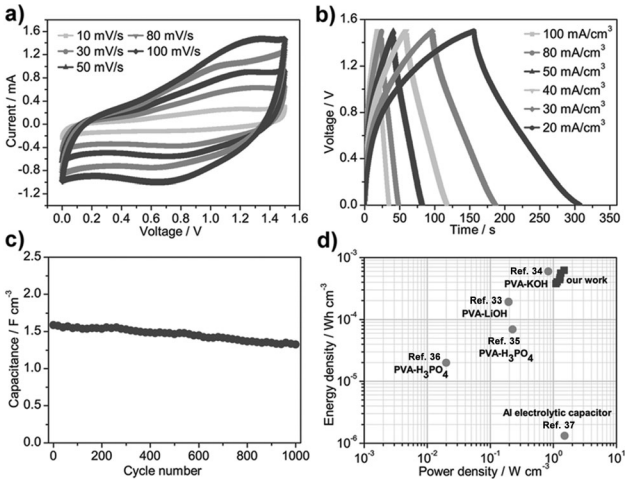

Figure 3. a) CV curves with scan rates between 10 and 100 mV s^{-1}, b) galvanostatic charge–discharge curves at current densities ranging from 20 to 100 mA cm^{-3} of the asymmetric supercapacitor in the potential window of 0.0–1.5 V. c) Cycling performance of the asymmetric supercapacitor at 40 mA cm^{-3}. d) Ragone plots of the asymmetric supercapacitor based on the full cell. The values reported for other supercapacitors are added for comparison. PVA = polyvinyl alcohol.

A charge–discharge cycling test was carried out to examine the long-term cyclability of the device (Figure 3c). During the cycling process at a current density of 40 mA cm^{-3}, a very small decrease of the capacitance was observed, which could have resulted from the consumption of the gel electrolyte caused by an irreversible reaction between the electrode material and the electrolyte.[32] The first ten charge–discharge cycles are shown in Figure S12. Good symmetry of both charge and discharge curves indicates superior capacitive behavior. After 1000 cycles, the device still maintained approximately 84% of its initial capacitance (1.59 F cm^{-3}), thus demonstrating the good cycling performance of the fiber-shaped all-solid-state supercapacitor. EIS measurements (EIS = electrochemical impedance spectroscopy) were performed to further evaluate the electrochemical performance of the supercapacitor (Figure S13). EIS measurements before and after 1000 cycles exhibited straight lines, thus showing ideal capacitive behavior. The equivalent series resistance (ESR) of the device decreased from 55.5 Ω before cycling to 46.3 Ω after cycling (see inset in Figure S13), which may be ascribed to the improved contact between the electrode material and the gel electrolyte after the cycling measurement. The result further demonstrates the exceptional electrochemical stability of the fiber-based asymmetric supercapacitor. The energy and power densities of the fiber-based all-solid-state asymmetric supercapacitor measured in the potential window of 0–1.5 V at different scan rates are shown in Figure 3d. With an operating potential of 1.5 V, we achieved a maximum volumetric energy density of 0.62 mW h cm^{-3} and power density of 1.47 W cm^{-3} for our asymmetric supercapacitors. Those values of our asymmetric supercapacitors are comparable or higher than those of all-solid-state asymmetric TiO_2@MnO_2//TiO_2@C and Co_9S_8//Co_3O_4/RuO_2 supercapacitors, symmetric PPy//PPy and SWCNT//SWCNT supercapacitors, and a 3 V/300 mF aluminum electrolytic capacitor.[33–37] This improved performance can be understood as an effect of the high ion permeability of the porous 3D architecture, the 3D ion and electron pathways on capacitive behavior, and the high cell voltage of 1.5 V.

However, the nickel fiber is too heavy and too hard to be used in light-weight and flexible devices. To develop a light-weight and flexible integrated photodetector system, we assembled a fiber-based flexible all-solid-state asymmetric supercapacitor using Co_3O_4 nanowires grown on titanium wire (with a diameter of 100 μm; see Figure S14) as positive electrode and carbon fibers/graphene as negative electrode, as the energy-supply device. Meanwhile, the graphene-on-carbon fibers were also used as light-sensitive material because of the high electron mobility and photon absorption over a wide wavelength range between visible and infrared.[38] Figure 4a shows a photograph as-fabricated fiber-based flexible asymmetric supercapacitor with effective lengths of 2.0 cm at different bending states. Figure 4b shows the CV curves of the flexible devices recorded at different scan rates in the potential window of 0.0–1.5 V. The current response depends on the potential, as opposed to the potential-independent current response of an electrochemical capacitor based on a non-Faradaic process, similar to the $Ni(OH)_2$/graphene//porous graphene asymmetric supercapacitor.[24]

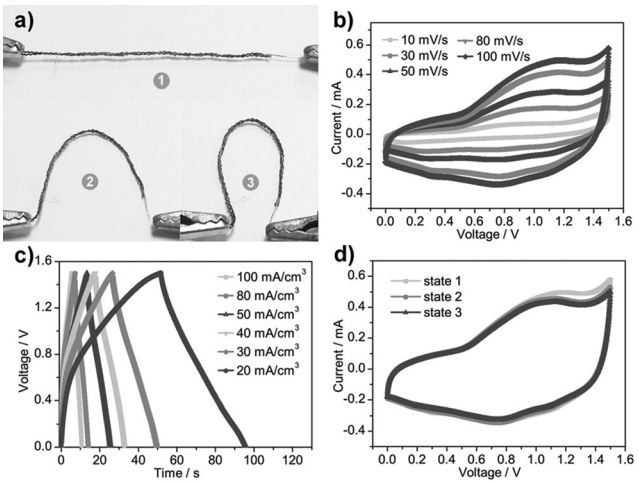

Figure 4. a) Photographs of the fiber-based all-solid-state flexible asymmetric supercapacitor at different bending states, b) CV curves, and c) galvanostatic charge–discharge curves of the flexible supercapacitor. d) CV curves obtained at a scan rate of 100 $mV s^{-1}$ at different bending states.

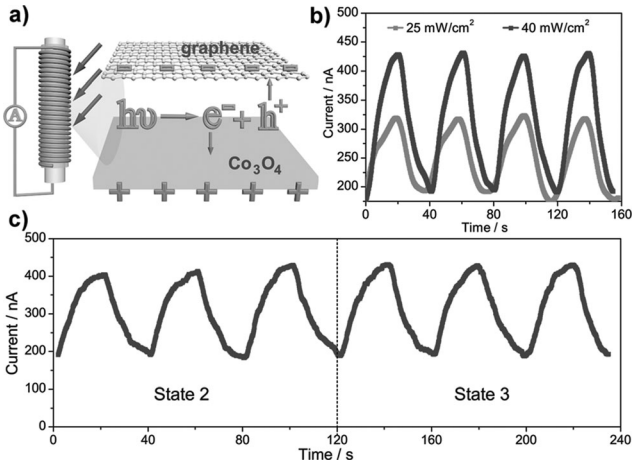

Figure 5. a) Schematic illustration of the integrated system. Current response of the photodetector powered by the flexible asymmetric fiber supercapacitor b) illuminated under different incident light intensities, and c) at different bending states under a light intensity of 40 $mW cm^{-2}$.

Figure 4c shows the galvanostatic charge–discharge profiles of the flexible asymmetric supercapacitor in the potential range of 0.0–1.5 V. As the current density increases, the capacitance of the device decreases because of the relatively insufficient Faradaic redox reaction in the fast charge–discharge processes. The flexibility of the fiber-based asymmetric supercapacitor was also investigated by carrying out CV measurements at 100 $mV s^{-1}$ in the normal (state 1) and the bent (states 2 and 3) state, corresponding to the states in Figure 4a. A negligible performance degradation shows the excellent mechanical stability and flexibility of these systems (Figure 4d). Furthermore, the high energy-storage performance and superior flexibility of the fiber-based all-solid-state asymmetric supercapacitors render them an unexceptionably flexible power source for flexible integrated photodetectors.

To demonstrate that the fiber-based asymmetric supercapacitor simultaneously acted as a photodetector, the internal mechanism of the integrated device was analyzed (Figure 5a). Upon the absorption of light, the electron–hole pairs generated in graphene would normally recombine in tens of picoseconds, depending on the quality and carrier concentration of the graphene.[39,40] However, when an external field that resulted from the fully charged supercapacitor was applied, the electron–hole pairs became separated, and the electrons moved to the positive Co_3O_4 electrode, and the holes to the negative graphene electrode, resulting in the improved leakage current of the supercapacitor. Therefore, photodetection may be accomplished by monitoring the changes of the leakage current. The leakage current of the supercapacitor was around 200 nA after about three hours (Figure S15). After the devices were charged to 1.5 V, the leakage currents of the device showed evident photoresponse when the graphene electrode was exposed to white light with an intensity of 25 and 40 $mW cm^{-2}$ (Figure 5b). After the light was turned off, the current returned to its initial value of about 200 nA. Asymmetric supercapacitors with Co_3O_4 on nickel fibers used as positive electrode also showed photodetection behavior (Figure S16). The increase of the leakage current under illumination by white light demonstrates that photodetection can be achieved with the integrated device.

The application of such integrated devices in flexible and wearable electronics largely depends on their flexibility (e.g. the flexibility of the supercapacitor and photodetector). Therefore, the photodetection performance of such an integrated device that was used as photodetector was tested with regard to its flexibility (Figure 5c). The performance changed little, thus demonstrating its excellent flexibility while maintaining its performance.

In conclusion, porous Co_3O_4 nanowires grown on a metal fiber were evaluated as the positive electrodes of fiber-based all-solid-state asymmetric supercapacitors with a high capacitance of 2.1 $F cm^{-3}$ at a current density of 20 $mA cm^{-3}$. These resulted from the large, electrochemically active surface of the porous nanostructures and the short paths for electron transport and ion diffusion of the 3D architectures. The potential window is improved from 0.6 V to 1.5 V, and the corresponding stored energy and delivered power are also enhanced at least by 1860% compared with that of the supercapacitor with a potential window of 0—0.6 V. More importantly, we successfully prepared a microscale flexible asymmetric supercapacitor using Co_3O_4 nanowires on titanium wire as positive electrode and graphene on carbon fibers as negative electrode, which are both flexible energy-storage device and flexible photodetector. The all-solid-state asymmetric supercapacitor exhibits a combination of both pseudocapacitive and EDLC-type properties, and little degradation of electrochemical performance, even when bent. Using a two-dimensional graphene layer as light-sensitive material, a high-performance flexible integrated photodetector can also be obtained. Thus, miniaturized flexible integrated

devices were fabricated that combine a supercapacitor and a photodetector on a single fiber.

Received: August 28, 2013
Revised: November 30, 2013
Published online: January 13, 2014

Keywords: flexibility · integrated photodetector · nanofibers · nanotechnology · supercapacitors

[1] Z.-H. Lin, G. Zhu, Y. S. Zhou, Y. Yang, P. Bai, J. Chen, Z. L. Wang, *Angew. Chem.* **2013**, *125*, 5169 – 5173; *Angew. Chem. Int. Ed.* **2013**, *52*, 5065 – 5069.
[2] Y. Yang, S. H. Wang, Y. Zhang, Z. L. Wang, *Nano Lett.* **2012**, *12*, 6408 – 6413.
[3] T. Chen, L. Qiu, Z. Yang, Z. Cai, J. Ren, H. Li, H. Lin, X. Sun, H. Peng, *Angew. Chem.* **2012**, *124*, 12143 – 12146; *Angew. Chem. Int. Ed.* **2012**, *51*, 11977 – 11980.
[4] W. Guo, X. Xue, S. Wang, C. Lin, Z. L. Wang, *Nano Lett.* **2012**, *12*, 2520 – 2523.
[5] J. Bae, Y. J. Park, M. Lee, S. N. Cha, Y. J. Choi, C. S. Lee, J. M. Kim, Z. L. Wang, *Adv. Mater.* **2011**, *23*, 3446 – 3449.
[6] Q. Yang, Y. Liu, Z. Li, Z. Yang, X. Wang, Z. L. Wang, *Angew. Chem.* **2012**, *124*, 6549 – 6552; *Angew. Chem. Int. Ed.* **2012**, *51*, 6443 – 6446.
[7] X. Wang, B. Liu, Q. Wang, W. Song, X. Hou, D. Chen, Y.-B. Cheng, G. Shen, *Adv. Mater.* **2013**, *25*, 1479 – 1486.
[8] Z. Zhan, L. Zheng, Y. Pan, G. Sun, L. Li, *J. Mater. Chem.* **2012**, *22*, 2589 – 2595.
[9] Y.-Q. Bie, Z.-M. Liao, H.-Z. Zhang, G.-R. Li, Y. ye, Y.-B. Zhou, J. Xu, Z.-X. Qin, L. Dai, D. P. Yu, *Adv. Mater.* **2011**, *23*, 649 – 653.
[10] W. Jin, Y. Ye, L. Gan, B. Yu, P. Wu, Y. Dai, H. Meng, X. Guo, L. Dai, *J. Mater. Chem.* **2012**, *22*, 2863 – 2867.
[11] T. Chen, Z. Yang, H. Peng, *ChemPhysChem* **2013**, *14*, 1777 – 1782.
[12] G. Q. Zhang, X. W. Lou, *Adv. Mater.* **2013**, *25*, 976 – 979.
[13] C. Guan, X. Li, Z. Wang, X. Cao, C. Soci, H. Zhang, H. J. Fan, *Adv. Mater.* **2012**, *24*, 4186 – 4190.
[14] G. Yu, L. Hu, M. Vosgueritchian, H. Wang, X. Xie, J. R. McDonough, X. Cui, Y. Cui, Z. Bao, *Nano Lett.* **2011**, *11*, 2905 – 2911.
[15] L. Hu, W. Chen, X. Xie, N. Liu, Y. Yang, H. Wu, Y. Yao, M. Pasam, H. N. Alshareef, Y. Cui, *ACS Nano* **2011**, *5*, 8904 – 8913.
[16] X. Wang, B. Liu, Q. Xiang, Q. Wang, X. Hou, D. Chen G. Shen, *ChemSusChem* **2013**, DOI: 10.1002/cssc.201300241.
[17] X. Xiao, T. Li, P. Yang, Y. Gao, H. Jin, W. Ni, W. Zhan, X. Zhang, Y. Cao, J. Zhong, L. Gong, W.-C. Yen, W. Mai, J. Chen, K. Huo, Y. L. Chueh, Z. L. Wang, J. Zhou, *ACS Nano* **2012**, *10*, 9200 – 9206.
[18] X. Xiao, X. Peng, H. Jin, T. Li, C. Zhang, B. Gao, B. Hu, K. Huo, J. Zhou, *Adv. Mater.* **2013**, *25*, 5091 – 5097.
[19] J. Bae, M. K. Song, Y. J. Park, J. M. Kim, M. Liu, Z. L. Wang, *Angew. Chem.* **2011**, *123*, 1721 – 1725; *Angew. Chem. Int. Ed.* **2011**, *50*, 1683 – 1687.
[20] Y. Fu, X. Cai, H. Wu, Z. Lv, S. Hou, M. Peng, X. Yu, D. Zou, *Adv. Mater.* **2012**, *24*, 5713 – 5718.
[21] J. Ren, L. Li, C. Chen, X. Chen, Z. Cai, L. Qiu, Y. Wang, X. Zhu, H. Peng, *Adv. Mater.* **2013**, *25*, 1155 – 1159.
[22] Y. Meng, Y. Zhao, C. Hu, H. Cheng, Y. Hu, Z. Zhang, G. Shi, L. Qu, *Adv. Mater.* **2013**, *25*, 2326 – 2331.
[23] V. T. Le, H. Kim, A. Ghosh, J. Kim, J. Chang, Q. A. Vu, D. T. Pham, J.-H. Lee, S.-W. Kim, Y. H. Lee, *ACS Nano* **2013**, *7*, 5940 – 5947.
[24] N. Liu, W. Ma, J. Tao, X. Zhang, J. Su, L. Li, C. Yang, Y. Gao, D. Golberg, Y. Bando, *Adv. Mater.* **2013**, *25*, 4925 – 4931.
[25] F. Zhang, C. Z. Yuan, X. J. Lu, L. J. Zhang, Q. Che, X. G. Zhang, *J. Power Sources* **2012**, *203*, 250 – 256.
[26] D. R. Rolison, J. W. Long, J. C. Lytle, A. E. Fischer, C. P. Rhodes, T. M. McEvoy, M. E. Bourg, A. M. Lubers, *Chem. Soc. Rev.* **2009**, *38*, 226 – 252.
[27] B. G. Choi, M. Yang, W. H. Hong, J. W. Choi, Y. S. Huh, *ACS Nano* **2012**, *6*, 4020 – 4028.
[28] Z. Tang, C.-H. Tang, H. A. Gong, *Adv. Funct. Mater.* **2012**, *22*, 1272 – 1278.
[29] J. Yan, Z. Fan, W. Sun, G. Ning, T. Wei, Q. Zhang, R. Zhang, L. Zhi, F. Wei, *Adv. Funct. Mater.* **2012**, *22*, 2632 – 2641.
[30] J. Ji, L. L. Zhang, H. Ji, Y. Li, X. Zhao, X. Bai, X. Fan, F. Zhang, R. S. Ruoff, *ACS Nano* **2013**, *7*, 6237 – 6243.
[31] L.-F. Chen, Z.-H. Huang, H.-W. Liang, Q.-F. Guan, S.-H. Yu, *Adv. Mater.* **2013**, *25*, 4746 – 4752.
[32] Y. Xiao, S. Kiu, F. Li, A. Zhang, J. Zhao, S. Fang, D. Jia, *Adv. Funct. Mater.* **2012**, *22*, 4052 – 4059.
[33] X. H. Lu, M. H. Yu, g. M. Wang, T. Zhai, S. L. Xie, Y. C. Ling, Y. X. Tong, Y. Li, *Adv. Mater.* **2013**, *25*, 267 – 272.
[34] J. Xu, Q. F. Wang, X. W. Wang, Q. Y. Xiang, B. Liang, D. Chen, G. Z. Shen, *ACS Nano* **2013**, *7*, 5453 – 5462.
[35] L. Y. Yuan, B. Yao, B. Hu, K. F. Huo, W. Chen, J. Zhou, *Energy Environ. Sci.* **2013**, *6*, 470 – 476.
[36] M. Kaempgen, C. K. Chan, J. Ma, Y. Cui, G. Gruner, *Nano Lett.* **2009**, *9*, 1872 – 1876.
[37] M. F. El-Kady, V. Strong, S. Dubin, R. B. Kaner, *Science* **2012**, *335*, 1326 – 1330.
[38] B. Chitara, L. S. Panchakarla, S. B. Krupanidhi, C. N. Rao, *Adv. Mater.* **2011**, *23*, 5419 – 5424.
[39] P. A. George, J. Strait, J. Dawlaty, S. Shivaraman, Mvs. Chandrashekhar, F. Rana, M. G. Spencer, *Nano Lett.* **2008**, *8*, 4248 – 4251.
[40] F. Rana, P. A. George, J. H. Strait, J. Dawlaty, S. Shivaraman, M. Chandrashekhar, M. G. Spencer, *Phys. Rev. B* **2009**, *79*, 115447.

